PROCEEDINGS OF SPIE

SPIEDigitalLibrary.org/conference-proceedings-of-spie

EUV photolithography mask inspection using Fourier ptychography

Antoine Wojdyla, Markus P. Benk, Patrick P. Naulleau, Kenneth A. Goldberg

Antoine Wojdyla, Markus P. Benk, Patrick P. Naulleau, Kenneth A. Goldberg, "EUV photolithography mask inspection using Fourier ptychography," Proc. SPIE 10656, Image Sensing Technologies: Materials, Devices, Systems, and Applications V, 106560W (29 May 2018); doi: 10.1117/12.2307860

SPIE.

Event: SPIE Commercial + Scientific Sensing and Imaging, 2018, Orlando, Florida, United States

Invited Paper

EUV photolithography mask inspection using Fourier ptychography

Antoine Wojdyla[a,b], Markus P. Benk[a], Patrick P. Naulleau[a], and Kenneth A. Goldberg[a,b]

[a]Center for X-Ray Optics, Lawrence Berkeley National Laboratory, Berkeley, CA (USA)
[a]Advanced Light Source, Lawrence Berkeley National Laboratory, Berkeley, CA (USA)

ABSTRACT

We use a synchrotron-based full-field EUV microscope with variable angle of illumination to perform Fourier ptychography reconstruction of patterned EUV photo-masks. We show that the reconstruction brings accurate quantitative phase information by comparing with through-focus data, and a 1.7-fold increase in resolution over the diffraction-limit by comparing with data acquired with larger numerical aperture. We also show how the complex-valued images reconstructed using Fourier ptychography can effectively be used for experiment-based computational lithography.

Keywords: x-ray optics, computational imaging, Fourier ptychography, synchrotron light source, EUV lithography, phase imaging, computational lithography, image processing

1. INTRODUCTION

The next generation in photolithography will make use of extreme ultraviolet radiations (EUV, wavelength λ=13.5 nm) to push further the limits of resolution imposed by diffraction effects. In this region of the spectrum, it is not possible to use conventional light sources and transmission optics. Therefore, optical systems developed for EUV lithography rely on reflective optics, and most importantly, the photomasks themselves operate in reflection. These photomasks are prone to optical effects that are unique to EUV lithography. Among these, the presence phase defects, caused by imperfections embedded in the mask substrate, requires new imaging techniques to better understand how they impact[1] wafer printing and how can they be mitigated. However, the optical phase imparted by an object is difficult to measure quantitatively: while microscopes which form the aerial images of a patterned mask only bring information about intensity, interferometric techniques are particularly difficult to implement at short wavelength. Still, it is possible to take advantage of the coherence properties of the illumination, where plane waves emanating from the object interfere with each other, to reconstruct a more accurate description of the object under investigation.

2. FOURIER PTYCHOGRAPHY

Fourier ptychography[2] is an imaging technique recently introduced in the visible range which is capable of reconstructing the complex angular spectrum of an object (corresponding to the Fourier transform of the complex electric field of the object) using a set of full-field images acquired with a microscope under coherent illumination. Under the Born approximation, these images all share an identical spectrum which is sampled differently by the numerical aperture of the objective lens (figure 1a.) By combining these images using an iterative phase retrieval algorithm (figure 1b), Fourier ptychography is capable of reconstructing the phase relation between the components of the angular spectrum, hence providing quantitative phase information about the sample, while at the same time synthesizing a larger numerical aperture from these images, thus increasing the effective resolution of the microscope.

Send correspondence to A.W; e-mail: awojdyla@lbl.gov, telephone: +1 (510) 486-6153

Image Sensing Technologies: Materials, Devices, Systems, and Applications V, edited by Nibir K. Dhar, Achyut K. Dutta, Proc. of SPIE Vol. 10656, 106560W · © 2018 SPIE
CCC code: 0277-786X/18/$18 · doi: 10.1117/12.2307860

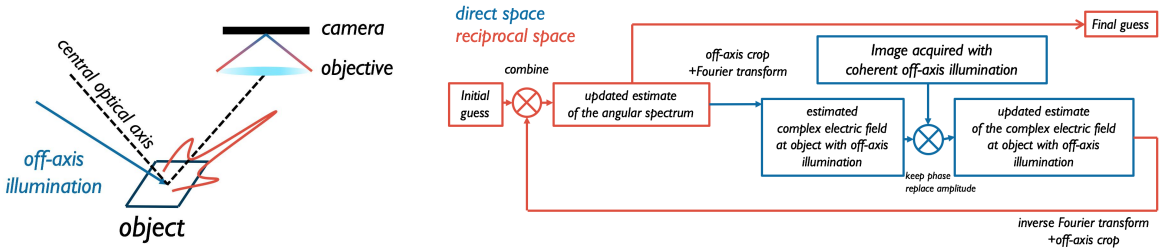

Figure 1. **Illumination diversity and Fourier Ptychography reconstruction.** (a) Depiction the off-axis illumination impact on the acquired image, and (b) Description of the Fourier ptychography reconstruction algorithm.

2.1 SHARP: A full-field EUV microscope with illumination diversity

The Sharp High-NA Reticle Review Project[3] (SHARP) is a synchrotron-based EUV microscope operating at a wavelentgth of 13.5 nm located at the Advanced Light Source, at Lawrence Berkeley National Laboratory. It is designed to emulate the aerial image formation in state-of-the-art EUV lithography scanners and allows the inspection of defects on EUV photomask using similar central ray angle (6°), numerical aperture, and illumination settings (including incoherent and dipole illumination.) The aerial image of the mask is formed on a CCD camera using an off-axis Fresnel zoneplate, typically providing a 900x magnification and a numerical aperture of .33 4xNA corresponding to NA=0.082 effective numerical aperture (the 4x term is here account for the 4x demagnification that occurs in a EUV lithography scanners; 1xNA and 4xCD respectively denotes the physical numerical apertures and critical dimensions on the mask.)

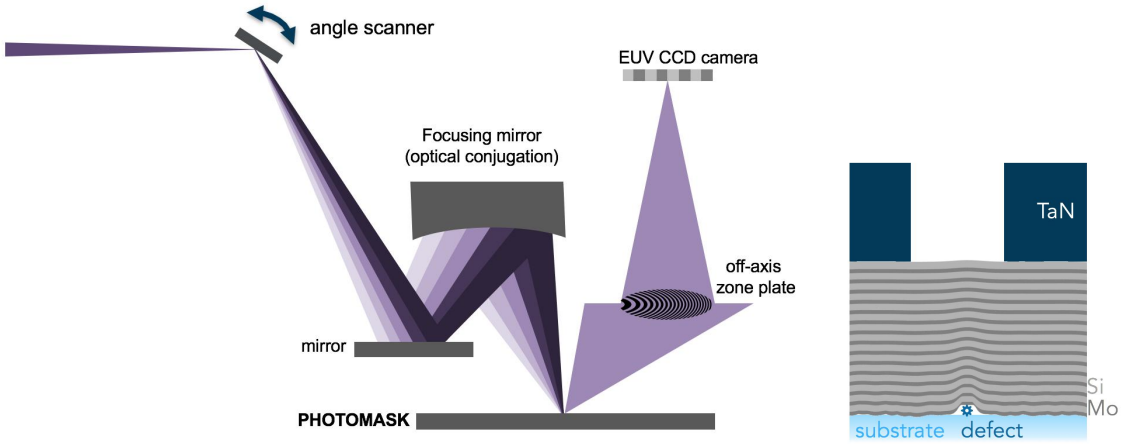

Figure 2. **Inspection of EUV photolithography masks** (a) Schematic of the SHARP EUV microscope, featuring a Fourier synthesis illuminator that allows illumination angle diversity by conjugating an angle scanner to the object plane. (b) Depiction of the structure of a typical EUV patterned photomask, where the reflective Mo/Si multilayer transfers the surface roughness and the occurrence of underlying defects on the substrate.)

The key element enabling Fourier ptychography with this microscope is its Fourier synthesis illuminator,[4] which consists in an angle scanner optically being conjugated with the object plane, using a condenser. The angle scanner is a MEMS device coated with a molybdenum/silicon reflective multilayer optimized for operation at 55°, providing a reflectivity of about 55% and capable of deflecting the incident beam by a about a ±1°, this angle later magnified 10x by the condenser, allowing off-axis illumination range up to 19° (figure 2a.) The objects imaged with the SHARP EUV microscope are usually standard 6″ patterned EUV photolithography masks, whose substrate is made of a quartz or ULE glass coated with a molybdenum/silicon multilayer (optimized for a central ray angle of 6° and providing 70% reflectivity, with a residual roughness of about 2Å), patterned with 70-nm thick TaN absorber (figure 2b.)

2.2 Experiments

We collected data on EUV photomasks using the .082 1xNA lens, with angle of illumination up to θ_{illum}=±3.76° in both direction around the central ray angle, corresponding to σ=0.8 in normalized pupil coordinate ($\sigma = \theta_{\text{illum}}/\text{NA}$; $\sigma > 1$ corresponding to dark-field imaging.) We have reconstructed the complex electric field at the object for patterns with various pitch, line-spacing and kinds of defects.

The first reconstructed object is a 112 nm-4xCD 1:1 line and space pattern on top of a severe phase defect (figure 3). We collected nine images with a maximum illumination angle of θ_{illum}=3.10°, yielding a resolution improvement of $(1+\sigma) = 1.66$ by synthesizing a 0.135NA aperture (corresponding to a larger coherent resolution limit of 0.5λ NA_{synth}= 50 nm-4xCD.) The phase defect can be characterized to bring a phase shift of ϕ=90°, indicative of effective height error of $h = \phi\lambda/4\pi = 1.5$ nm underneath the pattern, illustrating the exquisite sensitivity of EUV lithography to small phase defects.

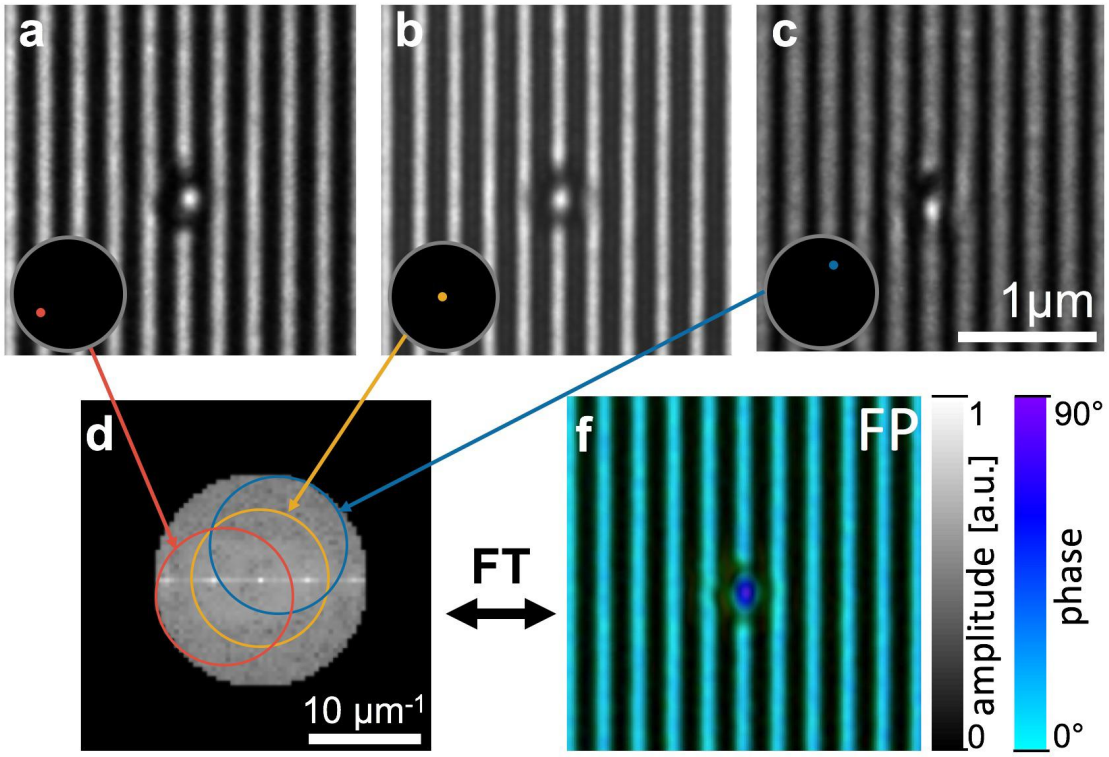

Figure 3. **Fourier ptychography reconstruction of a defect on a EUV photolithography mask.** (a-c) data acquired for various incidence angle up to 3.1° relative to the central ray angle (6°), as indicated in the insert relative to the normalized pupil coordinate; the arrows point to their contributions in the reconstructed angular spectrum (d) complex-valued angular spectrum, with a synthesized numerical aperture of 0.135NA (c) complex-valued electric field at the object from the Fourier ptychography reconstruction; the angular spectrum and the complex object form a Fourier-transform pair.

We have collected data on many other similar defects under the same conditions (figure 4.) These results are illustrative of the fact that defects can be amplitude defects, phase defects, or a mixture of phase and amplitude. Among these, (f) is a typical example of amplitude defect, while (g) is a typical example of a phase defect. Looking at a vast collection of defects, we found out that most of the defects flagged for actinic reviews were amplitude defects, suggesting that phase defects are less likely to be discovered by complementary means such as CD-SEM or DUV inspection.

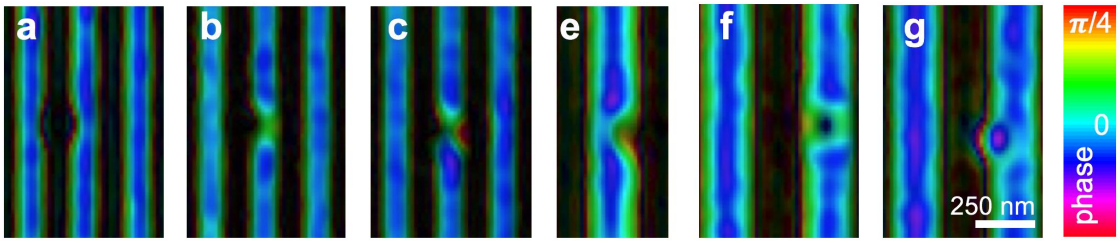

Figure 4. **Various kinds of defects found on EUV photo-mask and characterized with Fourier ptychography.** (a-g) Amplitude and phase of Fourier ptychography reconstructions from data acquired with a .33 4xNA lens. (f) is a typical example of amplitude defect, while (g) is a typical example of a phase defect.

3. EVALUATING THE FOURIER PTYCHOGRAPHY RECONSTRUCTION

In order to assess the validity of the Fourier ptychography reconstruction, we have compared these reconstructions with data acquired by other means. First, we have acquired through-focus data with the same 0.082NA lens, to compare the behavior of the phase, since phase controls the through-focus behavior of the pattern. The angular spectrum of the Fourier ptychography reconstruction pattern (reconstructed from intensity images with illumination angles up to θ_{illum}=3.76°, or σ=0.8) was first restricted to an equivalent numerical aperture of 0.082NA, to match the through-focus data (figure 5). By applying a quadratic phase corresponding to the defocus, we can see that the through-focus behavior of the aerial image can be faithfully reproduced, down to the speckle caused by the inherent roughness of the substrate.

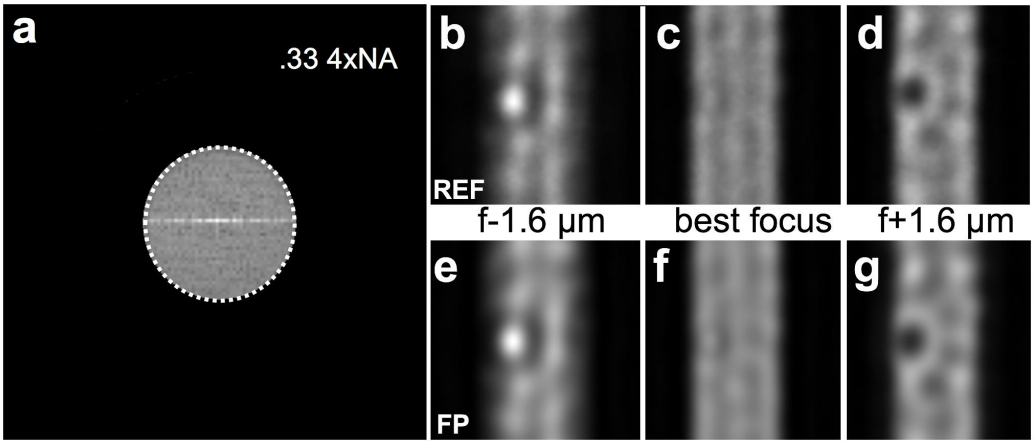

Figure 5. **Numerical refocusing at 0.082NA of a phase defect on a 500 nm-4xCD line.** (a) angular spectrum of the FP reconstruction (b-d) through-focus data acquired with a 0.082NA lens (e-g) numerical refocusing of the FP reconstruction (reconstructed from 0.082NA data with σ=0.8 maximum illumination angle.)

In order to assess the validity of the increase in resolution, we have collected through-focus data on the same pattern, but with a lens having a larger numerical aperture of 0.16NA. For practical reasons, the operating central ray angle of that lens is 10°. The same numerical refocusing was performed on the FP reconstruction, while limiting the effective numerical aperture to 0.16. The behavior of the through-focus data and the numerical refocusing do agree very well (figure 6), except for some shadowing effect caused by the difference in central ray angle.

Another test for the validity of the FP reconstruction is to look at the line-width roughness caused by the intrinsic roughness of the substrate;[5] this is important in EUV lithography, since this causes variations in the local critical-dimension uniformity (LCDU). We have reconstructed 224 nm-(4x)pitch lines using data acquired with σ=0.66, without including the central illumination in the reconstruction dataset, restricted the effective

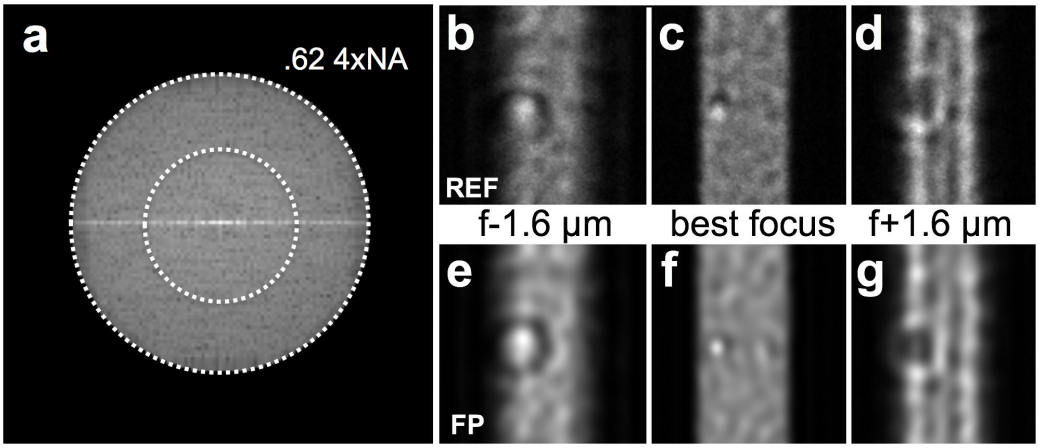

Figure 6. **Numerical refocusing at 0.16NA of a phase defect on a 500 nm-CD line.** (a) angular spectrum of the FP reconstruction (b-d) through-focus data acquired with a 0.16NA lens and 10deg central ray angle (e-g) numerical refocusing of the FP reconstruction (reconstructed from 0.082NA data with σ=0.8 maximum illumination angle at 6° central ray angle)

numerical aperture to 0.082NA and compared it the actual data acquired with a 0.082NA lens and central illumination (figure 7.) The variations of the line-width for the FP reconstruction and the original data are similar: the standard deviation of the difference between the two is 2.3 nm-rms, comparable to the contribution of the shot-noise expected for these experimental conditions (in the order of 1.5 nm-rms for 20 photons/pixels), and much smaller than the effective pixel size (15 nm) on the camera.

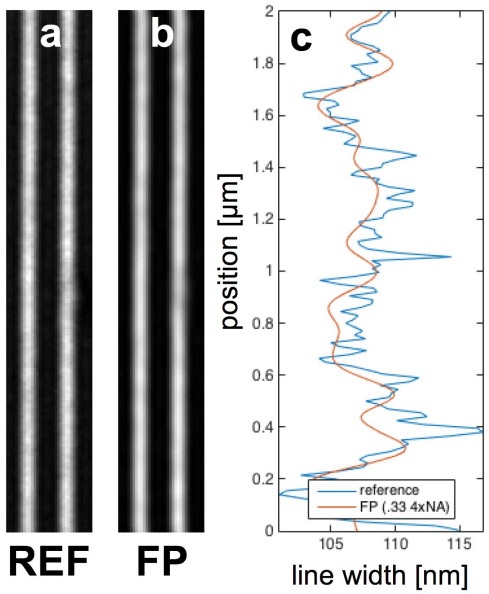

Figure 7. **Line-width roughness is accurately conserved in Fourier ptychography reconstructions.** (a) aerial image of 224 nm (1x)-pitch 1:1 line and space pattern acquired with a 0.082NA lens (b) synthesized aerial image from the Fourier ptychography reconstruction (acquired with a .082NA lens, and σ=±0.6 illumination, filtered down to .082NA) (c) line-width from both aerial images.

The fidelity of line-width roughness is an example of the advantage of Fourier ptychography (based on full-field microscope) over conventional ptychography,[6] where the LDCU information is often lost because of residual

motions of the stages. In the case of conventional ptychography, the reconstruction of the angular spectrum is made through the use of diffractograms acquired by moving the beam spot relative to sample. The relative positioning accuracy between two acquisition is typically in the order of 5 nm, responsible for a phase noise in the angular spectrum reconstruction that smears the edges. Fourier ptychography requires no moving parts between the object and the camera, and is thus very stable.

4. IMAGE SYNTHESIS USING THE ANGULAR SPECTRUM

Beyond defocusing, the reconstruction of the angular spectrum of the object allows extended manipulation of the information it contains (the angular spectrum should not be mistaken for the Fourier transform of the intensity of an image, which corresponds to the power spectral density (PSD) of the image.)

4.1 Numerical aperture synthesis

First, the FP reconstruction of the angular spectrum has a synthetic numerical aperture of $(1+\sigma)$ which can be restricted to a smaller, in order to emulate projection optics of smaller numerical aperture (figure 8) or even anamorphic imaging, where the pupil is ellipsoidal in shape.

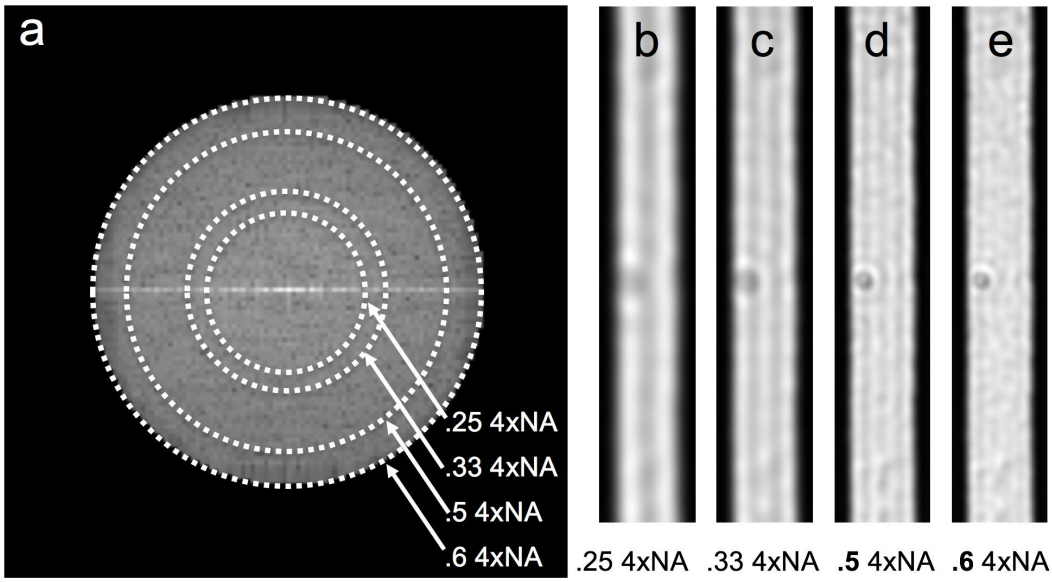

Figure 8. **Synthesis of numerical aperture of the optical system.** (a) angular spectrum of the object (b-e) corresponding aerial images for various restriction of the pupil size of the optical system.

4.2 Pupil function synthesis

Moreover, the knowledge of the angular spectrum of the object provides a comprehensive description of the object under study, and optical effects usually associated with complex objective lenses, such as Zernike phase contrast lenses (ZPC[7]), are straightforward to emulate, since they only require to apply a phase mask to the angular spectrum (figure 9). This is useful to improve the contrast of specific features, and could eventually be used in order to train a neural network to categorize defects, based on real data; the presence of substrate-induced speckle makes it superior to simulation.

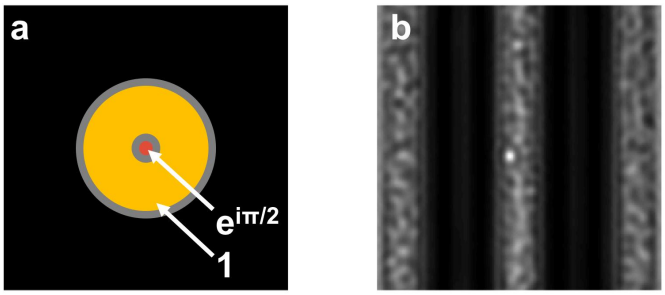

Figure 9. **Synthesis of a specialty lens.** (a) The pupil function can be modified to impose a $\pi/2$ phase shift between the specular beam (at the center of the pupil) and the rest of the angular spectrum, in order to emulate the effect of any Zernike phase contrast (ZPC) lens. (b) aerial image resulting in a $\pi/2$ ZPC (the pupil is limited to .33 4xNA)

4.3 Illumination synthesis

Since the (coherent) angular spectrum is wholly reconstructed, it is possible to emulate all kinds illumination settings, by incoherently summing individual contributions of various parts of the spectrum (figure 10). This can especially useful in the case of source-mask optimization, where the respective shape of the patterned feature and the illumination are matched to achieve better contrast (*e.g.* squareness of a contact, increased normalized image log-slope), or where additional features, such as sub-resolution assists,[8] can be added in order to improve the behavior of the aerial image through focus and optimize the process window.

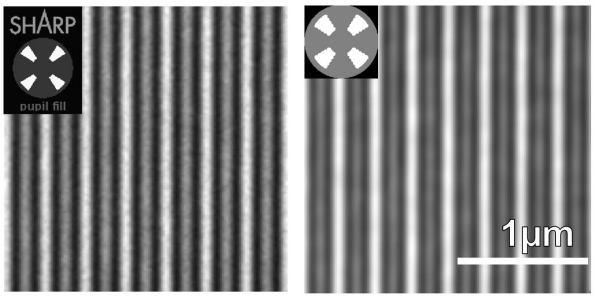

Figure 10. **Synthesis of illumination.** (a) Image of a line and space pattern with sub-resolution assist features under quasar illumination. (b) image with synthesized quasar illumination from a FP reconstruction (data acquired with coherent illumination and illumination angles corresponding to σ=0.8

5. CONCLUSION

We have demonstrated that Fourier ptychography can be adapted at small wavelength, where transmissive optical elements are excluded, on a fixed source that is a synchrotron. We have assessed the physical validity of the reconstructions. Whereas lithography is a field very concerned with diffraction-limited performances and extreme imaging conditions, we have seen no evidence of 3D-effects (due to the peculiar topology of EUV masks) that would negatively affect the Fourier ptychography reconstruction — all these effects seemingly captured by the angular spectrum representation of the object under study. We have also shown that manipulating the reconstructed angular spectrum can be useful for a wide variety of studies concerned with the optical properties of EUV photolithography mask.

ACKNOWLEDGMENTS

The SHARP microscope was funded by SEMATECH and this work was performed by Lawrence Berkeley National Laboratory under the auspices of the U.S. Department of Energy. The Advanced Light Source is supported by

the Director, Office of Science, Office of Basic Energy Sciences, of the U.S. Department of Energy under Contract No. DE-AC02-05CH11231.

REFERENCES

[1] Mangat, P., Verduijn, E., Wood, O. R., Benk, M. P., Wojdyla, A., and Goldberg, K. A., "Mask blank defect printability comparison using optical and SEM mask and wafer inspection and bright field actinic mask imaging," in [*Proc. of SPIE*], **9658**, 96580E (2015).

[2] Zheng, G., Horstmeyer, R., and Yang, C., "Wide-field, high-resolution Fourier ptychographic microscopy," *Nature Photonics* **7**, 739–745 (jul 2013).

[3] Goldberg, K. A., Mochi, I., Benk, M. P., Allezy, A. P., Dickinson, M. R., Cork, C. W., Zehm, D., Macdougall, J. B., Anderson, E. H., Salmassi, F., Chao, W. L., Vytla, V. K., Gullikson, E. M., DePonte, J. C., Jones, M. S., Van Camp, D., Gamsby, J. F., Ghiorso, W. B., Huang, H., Cork, W., Martin, E., Van Every, E., Acome, E., Milanovic, V., Delano, R., Naulleau, P. P., and Rekawa, S. B., "Commissioning an EUV mask microscope for lithography generations reaching 8 nm," in [*Extreme Ultraviolet (EUV) Lithography IV*], Naulleau, P. P., ed., **8679**, 867919–867919–10 (apr 2013).

[4] Naulleau, P. P., Goldberg, K. A., Batson, P., Bokor, J., and Denham, P. E., "Fourier-synthesis custom-coherence illuminator for extreme ultraviolet microfield lithography," *Applied Optics* **42**(5), 820–826 (2003).

[5] Wojdyla, A., Donoghue, A., Benk, M. P., Naulleau, P. P., and Goldberg, K. A., "Aerial imaging study of the mask-induced line-width roughness of EUV lithography masks," in [*Proc. of SPIE*], **9776**, 97760H (2016).

[6] Seaberg, M. D., Zhang, B., Gardner, D. F., Shanblatt, E. R., Murnane, M. M., Kapteyn, H. C., and Adams, D. E., "Tabletop nanometer extreme ultraviolet imaging in an extended reflection mode using coherent Fresnel ptychography," *Optica* **1**, 39 (jul 2014).

[7] Wang, Y.-G., Miyakawa, R., Chao, W. L., Benk, M., Wojdyla, A., Donoghue, A., Johnson, D., Goldberg, K. A., Neureuther, A., Liang, T., and Naulleau, P., "Enhancing defect detection with Zernike phase contrast in EUV multilayer blank inspection," in [*Proc. of SPIE*], **9422**, 94221C (2015).

[8] Burkhardt, M. and Raghunathan, A., "Best focus shift mechanism for thick masks," in [*Proc. SPIE*], Wood, O. R. and Panning, E. M., eds., 94220X (mar 2015).